

# First-principles calculations of graphene nanoribbons in gaseous environments: Structural and electronic properties

M. Vanin, J. Gath, K. S. Thygesen, and K. W. Jacobsen  
*Center for Atomic-scale Materials Design, Department of Physics*  
*Technical University of Denmark, DK - 2800 Kgs. Lyngby, Denmark*  
 (Dated: October 27, 2010)

The stability of graphene nanoribbons in the presence of typical atmospheric molecules is systematically investigated by means of density functional theory. We calculate the edge formation free energy of five different edge configurations passivated by H, H<sub>2</sub>, O, O<sub>2</sub>, N<sub>2</sub>, CO, CO<sub>2</sub>, and H<sub>2</sub>O, respectively. In addition to the well known hydrogen passivated armchair and zig-zag edges, we find the edges saturated by oxygen atoms to be particularly stable under atmospheric conditions. Saturation of the zigzag edge by oxygen leads to the formation of metallic states strictly localized on the oxygen atoms. Finally, the vibrational spectrum of the hydrogen and oxygen passivated ribbons are calculated and compared.

PACS numbers: 73.20.At, 73.22.Pr, 71.15.Mb

## I. INTRODUCTION

Graphene, a single atomic carbon layer, has attracted extensive research interests in the last few years<sup>1-4</sup>. Recent advances in experimental techniques have lead to the fabrication of several graphene-based structures for both fundamental physics investigations and promising applications. Graphene nanoribbons (GNRs), in particular, have received considerable attention due to their possible role in future carbon-based nanoelectronics<sup>5,6</sup>. GNRs are graphene strips of finite width, in which lateral confinement opens an electronic gap as opposed to the vanishing gap in infinite graphene sheets.

Theoretical calculations and experiments have shown that the electronic and transport properties of GNRs are strongly influenced by the actual atomic configuration of the edges<sup>7</sup> which, contrary to bulk graphene, are very reactive. A detailed knowledge of the stability and electronic properties of the different types of edges is therefore required in order to understand and ultimately design GNRs with specific properties.

Most theoretical calculations on GNRs have considered the the armchair and zigzag edges with or without hydrogen passivation. However, recent calculations have shown that other edge configurations can also show high stability<sup>8</sup>. Since molecular hydrogen is one of the most common contaminants even in ultra high vacuum experiments, it is certainly relevant to consider its influence at the edges<sup>9</sup>. On the other hand, especially at room temperature and under ambient conditions, the effect of other gas molecules on the edge stability should also be considered. This is also relevant from the perspective of chemical functionalization<sup>10,11</sup>.

In this paper, we study the stability of five different edge geometries in the presence of H<sub>2</sub>, O<sub>2</sub>, N<sub>2</sub>, CO, CO<sub>2</sub> and H<sub>2</sub>O using first principles calculations. The different edge geometries for the pristine ribbons with the corresponding abbreviations are shown in Fig. 1. We find that the edges passivated by atomic oxygen are the most stable under atmospheric conditions closely followed by the

zig-zag and armchair edges with hydrogen adsorbed. The oxygen passivated zig-zag GNR is found to be metallic with the states at the Fermi level strictly localized on the oxygen *p* orbitals. The vibrational spectrum of the hydrogen and oxygen passivated GNRs are calculated and discussed. Throughout the paper we focus on free-standing graphene and thus neglect any effect related to the substrate. Whether this is a reasonable assumption clearly depends on the strength of the substrate-graphene interaction. This is likely to make the edges less reactive towards gas species, since the edges would be already stabilized by the chemical bond to the substrate. For metallic substrates the nature of the substrate-graphene interaction is still unclear, but DFT calculations indicate that it can vary considerably depending on the metal<sup>12,13</sup>.

## II. COMPUTATIONAL DETAILS

Density functional theory (DFT) calculations are performed with the GPAW code<sup>14,15</sup> which is a real space implementation of the the projector augmented wave method<sup>16</sup>. The widths of the nanoribbons are in the range 20 – 23 Å, corresponding to 10-12 carbon dimers, which is needed in order to get fully converged results with respect to the width. Note that this size is also relevant to modern experiments, where sub-10nm wide GNRs are now achieved<sup>5,6</sup>. The GNRs are separated by 10 Å in all directions. All calculations are spin-polarized and use the RPBE<sup>17</sup> exchange-correlation functional. A grid-spacing of 0.18 Å is used, and a (1×1×10) Monkhorst-Pack *k*-point grid is employed to sample the Brillouin zone along the periodic direction of the nanoribbons. We relax all the structures until the maximum force is lower than 0.05 eV/Å.

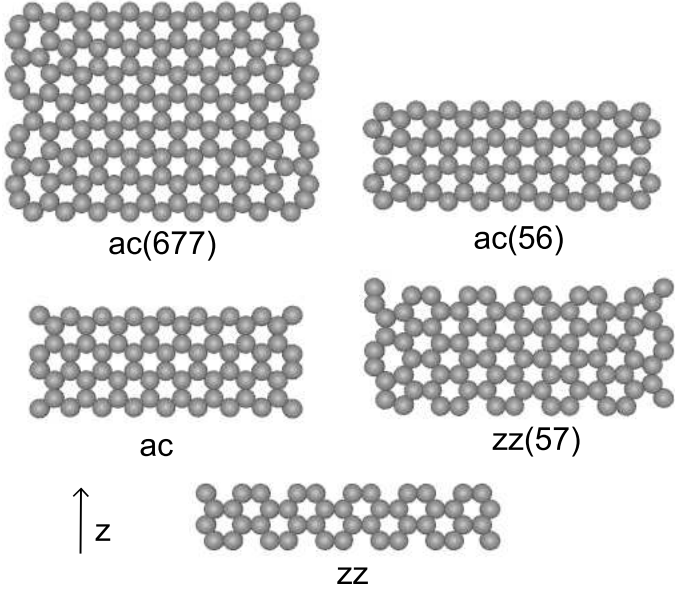


FIG. 1: The standard and reconstructed edge geometries (and corresponding abbreviations) considered in this study. The figures show two unit cells of the nanoribbons with periodicity along the  $z$ -direction.

	H	O <sub>2</sub> <sup>diss</sup>	O <sub>2</sub>	N <sub>2</sub> <sup>diss</sup>	N <sub>2</sub>	CO	H <sub>2</sub> O	CO <sub>2</sub>
ac(677)	-2.59	-4.33	-0.45	0.86	-0.22	-0.97	-1.46	0.66
ac(56)	-5.36	-9.88	-3.22	-1.95	-1.25	-3.03	-2.49	-0.20
zz(57)	-2.99	-5.13	-3.09	0.14	0.96	-1.05	-2.24	-0.82
ac	-3.99	-4.90	-1.29	1.73	0.44	-2.31	-2.56	-0.86
zz	-5.19	-7.44	-0.96	0.05	0.20	-1.42	-0.85	0.65

TABLE I: Numerical values of the adsorption energies,  $E_{\text{ads}}$ , corresponding to Fig. 2. All values are in eV.

### III. STABILITY

#### A. Adsorption energies

For each of the five edge configurations we calculate the adsorption energy of the different molecules according to

$$E_{\text{ads}} = E^{\text{ribb}+\text{mol}} - N_{\text{mol}}E^{\text{mol}} - E^{\text{ribb}} \quad (1)$$

where  $E^{\text{ribb}+\text{mol}}$  is the total energy of the ribbon with the adsorbed gas molecule,  $N_{\text{mol}}$  is the number of adsorbed molecules,  $E^{\text{mol}}$  is the total energy of the molecule in the gas phase and  $E^{\text{ribb}}$  is the total energy of the pristine ribbon. In order to avoid the erroneous DFT description of the O<sub>2</sub> gas-phase triplet groundstate, we use H<sub>2</sub>O and H<sub>2</sub> as suggested in Ref. 18. The adsorption energies are summarized in Fig. 2 and shown in I.

It can be seen that saturation by oxygen is the most favorable for all edge configurations. We note that this is in agreement to Ref. 19 in which the authors conclude

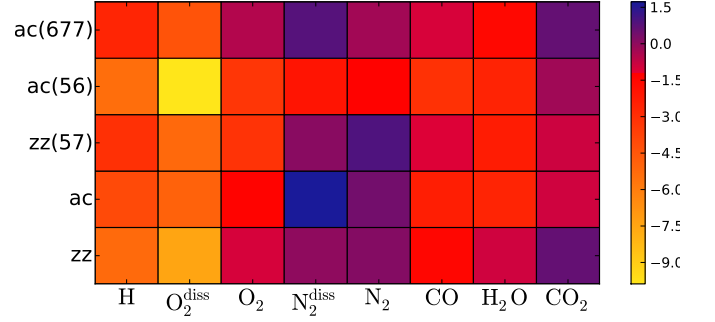


FIG. 2: (Color online) Adsorption energy,  $E_{\text{ads}}$ , for the different molecular species on the different edge configurations in eV. In the case of nitrogen and oxygen we have considered both the molecular and dissociated forms on the edge. In all cases the adsorption energy is given per *molecule*.

that zig-zag nanoribbons are more likely to be oxidized than hydrogenated.

While the high reactivity of the zig-zag edge is well established<sup>20</sup>, we also find the ac(56) to be very reactive; in fact for several species this is the most reactive edge configuration. As for the zig-zag edge, the origin of the high reactivity of the ac(56) edge is a (spin polarized) peak in the density of states close to the Fermi energy. Consistent with their high reactivities, the pristine zz and ac(56) edges also have the highest edge formation energies (see Table II), i.e. they are the least stable edges in the absence of molecular gas species.

Finally, we note that all the reported results are for adsorption at the edge carbon atoms since these are by far the most reactive sites. For example we find that H adsorption on a carbon atom located next to the edge is already unfavorable compared to H<sub>2</sub> in the gas phase.

#### B. Edge formation energies

The adsorption energies discussed in the previous section are relevant once a given edge configuration has been formed. More generally, to thermodynamic stability of an edge in the presence of gas molecules should also take the energetic cost of forming the edge into account. To calculate the edge formation free-energy we first calculate the formation energy of the pristine edges,

$$E_{\text{f}} = \frac{1}{2L} (E^{\text{ribb}} - N_{\text{C}}E^{\text{bulk}}) \quad (2)$$

where  $E^{\text{ribb}}$  is the total energy of a ribbon with  $N_{\text{C}}$  carbon atoms in the supercell and  $E^{\text{bulk}}$  is the total energy per atom in bulk graphene. Our calculated energies shown in Table II are in very good agreement with Ref. 8. We remark, that for pristine GNRs the zz(57) reconstruction has the lowest edge energy.

The adsorption energy  $E_{\text{ads}}$  is used to obtain a free-energy by taking into account the chemical potential,

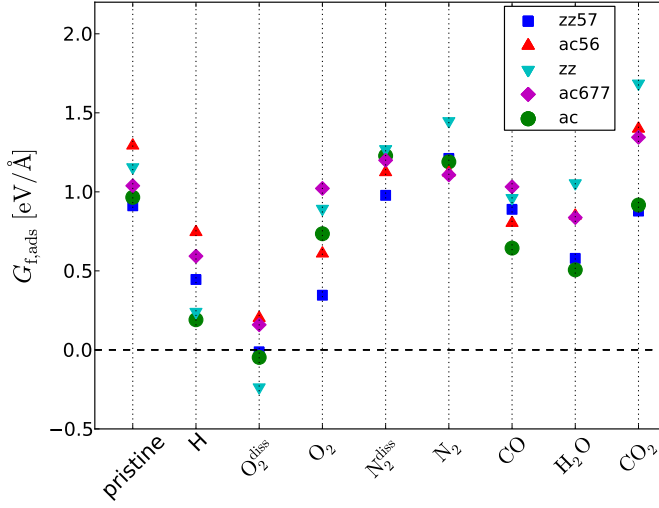


FIG. 3: (Color online) Edge formation free energy of graphene nanoribbons with different edge structures (different symbols) and different adsorbed molecules at the edge. The free energy is evaluated at 300K. The pressure for each structure with a given adsorbate is taken to be the partial pressure of the gas-phase adsorbate at atmospheric conditions.

$\mu_{\text{gas}}$ , of the gas at a given temperature and pressure

$$G_{\text{ads}} = \frac{1}{L} E_{\text{ads}} - \rho_{\text{gas}} \mu_{\text{gas}} \quad (3)$$

where  $\rho_{\text{gas}} = N_{\text{mol}}/L$  is the density of adsorbed species. The chemical potential at temperature  $T$  and partial pressure  $P$  is given by

$$\mu = H^0(T) - H^0(0) - TS^0(T) + k_B T \ln \left( \frac{P}{P^0} \right) \quad (4)$$

where  $H^0$  and  $S^0$  are enthalpies and entropies of the gas phase molecules at  $P^0 = 1$  bar.

Finally, the edge formation free-energy in the presence of adsorbates is obtained as

$$G_{\text{f,ads}} = E_{\text{f}} + G_{\text{ads}} \quad (5)$$

The vibrational contributions to  $G_{\text{f,ads}}$  are not included since they are expected to be insignificant<sup>21</sup>.

Fig. 3 summarizes the calculated edge formation free-energies at 300K and atmospheric partial pressures for the different gas species. The qualitative picture does not change if the temperature and pressure ranges are varied within experimentally accessible ranges. The results are also reported in Table II together with the edge formation energies calculated at 0K. It is immediately apparent that edges saturated by atomic oxygen are the most stable. In particular, the lowest energy configurations are the standard zigzag and armchair, followed by the reconstructed zz(57); the other reconstructed edges are generally less stable. This agrees with Ref. 9 where hydrogen passivation was considered. The armchair and

	zz(57)		ac		ac(56)		zz		ac(677)	
	300K	0K	300K	0K	300K	0K	300K	0K	300K	0K
pristine		0.92		0.96		1.30		1.16		1.04
H	0.46	0.30	0.21	0.03	0.75	0.66	0.25	0.10	0.61	0.43
O	0.00	-0.13	-0.03	-0.19	0.21	0.13	-0.22	-0.36	0.17	0.02
N	0.98	0.93	1.24	1.17	1.13	1.06	1.28	1.17	1.21	1.14
CO	0.90	0.70	0.66	0.42	0.82	0.58	0.99	0.58	1.05	0.81
N <sub>2</sub>	1.22	1.11	1.20	1.07	1.14	1.00	1.47	1.24	1.12	0.99
O <sub>2</sub>	0.42	0.28	0.82	0.66	0.69	0.54	1.03	0.77	1.06	0.99
H <sub>2</sub> O	0.59	0.46	0.52	0.36	0.87	0.71	1.09	0.81	0.86	0.70
CO <sub>2</sub>	0.89	0.75	0.93	0.76	1.42	1.25	1.71	1.42	1.36	1.19

TABLE II: Edge formation free-energy at 0K and 300K for the different nanoribbons and adsorbed species. All energies are in eV/Å.

zigzag edges saturated by hydrogen are also quite stable thus making H and O saturations the most stable ones. For this reason we will focus in particular on the oxygen saturated GNR, i.e. the most stable one, in the rest of the paper. Note that the negative formation free-energies for some of the oxygen saturated edges mean that a graphene sheet will spontaneously break in order to generate edges and lower its energy. However one needs to be careful in analyzing these results, since significant energy barriers may be involved in the process and they are not included in our study. Furthermore, once the oxygen molecule has dissociated, atomic oxygen is also reactive on the planar graphene sheet (3.23 eV compared to atomic oxygen<sup>22</sup>), thus making the dynamics of the dissociated oxygen potentially very complicated. Oxygen saturated edges were also found to be the most stable in another study<sup>23</sup>, where the authors also consider edge configurations beyond saturation by a single atom.

In addition to H and O, the adsorption of H<sub>2</sub>O and CO is also found to stabilize most edges. In the case of H<sub>2</sub>O, the dissociation of the water molecule is always energetically favoured compared to the molecular adsorption. In particular, it dissociates into OH and H on ac, ac(56), zz(57) and ac(677). On the zz edge, instead, H<sub>2</sub>O spontaneously dissociates into an adsorbed oxygen at the edge and releasing the two hydrogen atoms in the gas phase. Nitrogen species and CO<sub>2</sub> bind rather weakly or not at all on all edge configurations.

These calculated data can furthermore be used in order to construct phase diagrams as a function of the chemical potential of a given gas species. This might be relevant for guiding experimental investigations in which GNRs are studied in the presence of a given gas species. An example is shown in Fig. 4 for the case of dissociated oxygen at the edges. This shows that for any experimentally accessible pressure of O<sub>2</sub>, the most stable edge configuration is the standard zig-zag, saturated by oxygen.

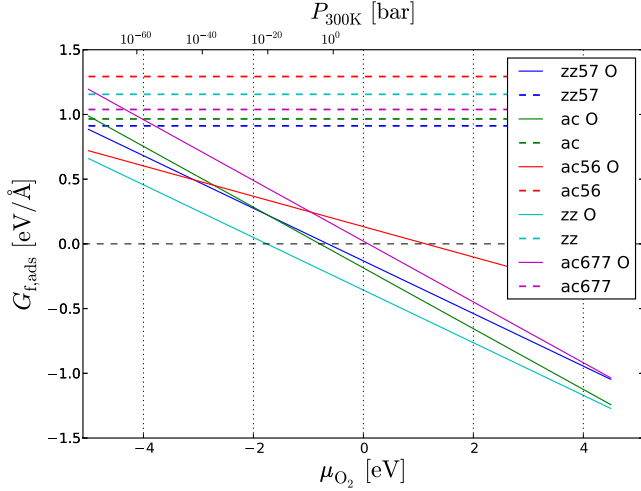


FIG. 4: (Color online) Edge formation free-energy for the different edge configurations of a graphene nanoribbon in a background of  $O_2$  gas.

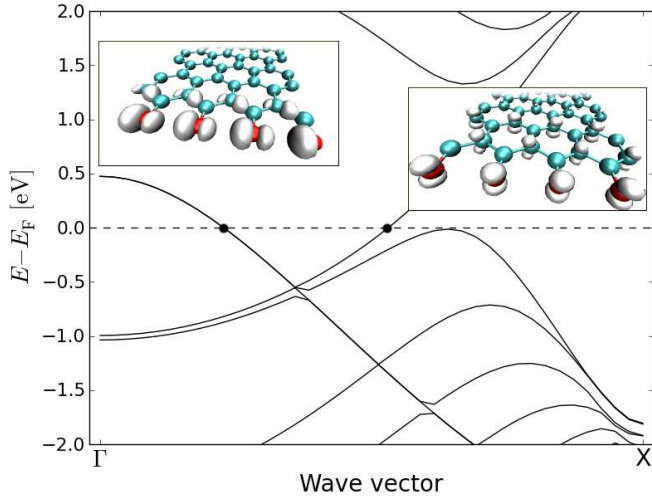


FIG. 5: (Color online) Band structure of a 22 Å wide zig-zag GNR saturated with O. The two insets show the states corresponding to the bands crossing the Fermi level, marked with black circles.

#### IV. OXYGEN SATURATED ZIG-ZAG EDGE

In the previous section we found that the zig-zag GNR saturated by atomic oxygen is the most stable thermodynamically. For this reason, we investigate in this section the ground state and vibrational properties of the oxygen passivated zig-zag GNR and compare it to the well studied hydrogen passivated case.

##### A. Bandstructure

Fig. 5 shows the Kohn-Sham band structure for the oxygen saturated GNR calculated with the RPBE func-

tional. Contrary to the hydrogen saturated case, its ground state is spin-paired and metallic. The states at the Fermi level are localized at the edges, and they have weight on the  $p$  orbitals of the oxygen atom. One state has  $p_z$  symmetry and it decays into the GNR away from the edge with weight on only one carbon sublattice (left inset of Fig. 5). The other state is almost completely localized on the out of plane  $p$  oxygen orbital (right inset of Fig. 5). This is also in contrast to the hydrogen saturated case, where the edge states are entirely localized on the edge carbon atoms.

##### B. Vibrational properties

Low energy spectroscopies probing the vibrational excitations have traditionally been a powerful tool for structure determination in molecules. It has recently become possible to study differences in the edge orientation of GNRs using Raman spectroscopy<sup>24,25</sup>. In view of this we have calculated the vibrational spectrum of the zig-zag GNRs passivated by hydrogen and oxygen in order to identify features specific to these types of edges.

###### 1. Computational details

To obtain the phonon frequencies we first compute the dynamical matrix in real space. The latter is obtained by numerical differentiation of the forces. A careful procedure to obtain the equilibrium configuration is found essential in order to obtain an accurate description of the phonon frequencies. Thus, for a single unit of the zzGNR, we used a grid spacing of 0.1 Å and a  $k$ -point sampling of  $(1 \times 1 \times 10)$ . The relaxation of the equilibrium structure is continued until the maximal residual forces are less than 0.02 eV/Å.

The dynamical matrix is evaluated in a supercell containing seven primitive cells of the GNR. All atoms in one of the primitive cells are displaced by  $\pm 0.02$  Å in the  $x$ ,  $y$ , and  $z$  directions (a total of  $6 \times N$  calculations) and the forces on all remaining atoms within a truncation radius of 7 Å of the displaced atom are stored. This requires a total of  $6 \times N$  calculations where  $N$  is the number of atoms in a primitive cell. For these calculations we use a grid spacing of 0.18 Å and a  $1 \times 1 \times 3$   $k$ -point sampling. We have verified that our results have converged with respect to these parameters and the truncation radius. The real space dynamical matrix is obtained from a finite difference of the forces, and the eigenvectors and frequencies are obtained after Fourier transformation.

###### 2. Results

The GNRs are finite in their width direction and thus they are subject to boundary conditions similar to that of a string with free ends. The edges therefore only allow

standing waves perpendicular to the ribbon axis and the phonon wave vector for a GNR consisting of  $N$  carbon dimers will be quantized as  $q_{\perp,n} = \pi n/w$ , where  $w$  is the width of the dimers and  $n = 0, \dots, N-1$  each corresponding to a normal mode. The dispersion relations therefore consist of six fundamental modes each with  $(N-1)$  overtones. A study of the  $\Gamma$ -point spectrum according to this classification has been done in a previous study<sup>26</sup> for hydrogen saturated nanoribbons with purely zigzag and armchair edges. The modes can be separated into the three categories according to their longitudinal, transverse, and out-of-plane nature. It is straightforward to identify which category a particular mode belongs to by weighting each of the three different spatial entries in the polarisation vector relative to its total norm. Each of the spatial categories can be separated into acoustical and optical parts giving rise to six series. The  $\Gamma$ -point spectrum is found to be similar to hydrogen saturated ribbons where a splitting into optical (160-200)meV and acoustical modes (0-160)meV is observed, as shown in Fig. 6. The transverse acoustical modes are seen to follow a near perfect  $1/\sqrt{w}$  behaviour which is understood in terms of the ribbon acting as a spring perpendicular to its axis with fixed spring constant.

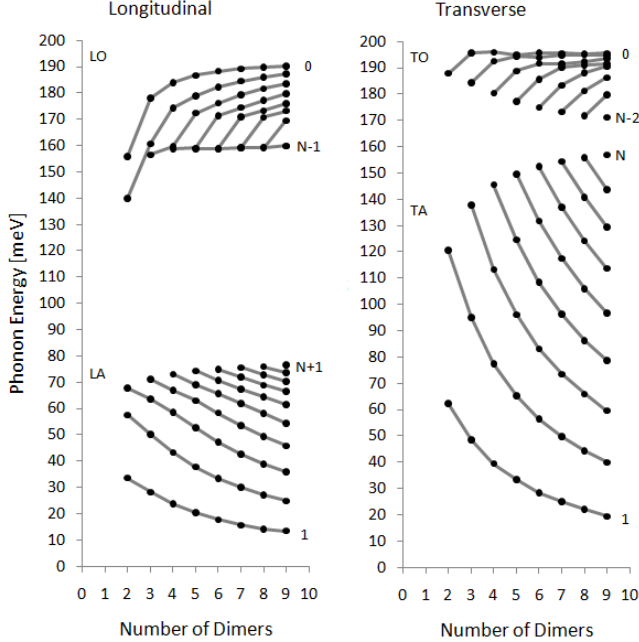


FIG. 6: The longitudinal (left) and transverse (right)  $\Gamma$ -point spectrum of the oxygen saturated zigzag nanoribbon as function of the number of carbon dimers. The fundamental mode of the acoustical series is zero for all widths and is not shown.

A separation of modes associated with the saturation atoms are not as simple in the case of oxygen as it is for hydrogen. Contrary to the hydrogen passivated ribbons where three degenerate pairs of edge localized modes are found at 380meV, 150meV and 125meV, only one local-

ized degenerate pair of carbon-oxygen modes shows up, namely the degenerated stretching modes (transverse direction). Similarly to the hydrogen passivated case, this pair is found to be independent of the ribbon width and is located around 182meV, except for the very narrow ribbons ( $N < 4$ ) where it is slightly higher. The last four modes are not separated from the remaining modes as for the case of hydrogen. In fact, the oxygen atoms participate as a continuation of the carbon system and enters in the bulk vibrational modes giving rise to two additional acoustical modes in the longitudinal series and the out-of-plane series. This coupling to the acoustical modes is understood in terms of the comparable masses of the two species. Also, for the transverse series one finds that an optical mode has been converted into an additional acoustical one. The optical modes of the longitudinal and out-of-plane series on the contrary remains similar to what is found for the hydrogen saturated ribbons, that is, the series are constituted of normal modes only coming from the carbon atoms.

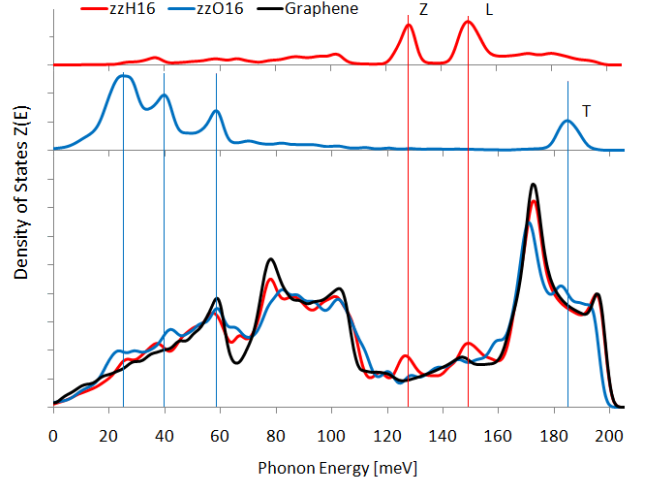


FIG. 7: (Color online) The total vibrational density of state of the 16 dimer wide (33Å) hydrogen(red) and oxygen(blue) saturated zigzag nanoribbon in comparison with graphene(black). The density of states weighted on the saturating atoms shown for the hydrogen and oxygen saturated 16 dimer zigzag ribbon, respectively.

The total vibrational density of states of the 16 dimer wide zigzag ribbon is obtained by integration in the  $\Gamma K M$ -direction and is shown in Fig. 7. Note that it represents the whole spectrum of states and not just the  $\Gamma$ -phonons. Except for some distinct peaks the total density of states for the hydrogen and oxygen saturated ribbons represents that of graphene fairly well. In order to compare the deviations in the density of states associated with the edge, the states localised on the edges have been separated out for each of the saturating species. The peaks present in the edge contribution are to a large degree recognisable in the corresponding total density of states spectrum. For the hydrogen saturated rib-

bon, the two peaks observed are the vibrational mode perpendicular to the carbon-hydrogen bond and out-of-plane mode. For the oxygen saturated ribbon only the transverse carbon-oxygen has a truly edge-localized vibrational pattern while the peaks observed in the acoustical part of the spectrum originates from individual normal modes in the longitudinal and out-of-plane series.

## V. CONCLUSION

As a general reminder, it should be noted that the results in this study do not consider the effects of the substrates. In most experiments, GNRs are grown or deposited on a substrate, which might affect the energetics at the edges. The interaction of the substrate with graphene edges is likely to be much stronger than the interaction with the bulk graphene<sup>12,13</sup>.

In conclusion we have studied the adsorption of common gas molecules at the edge of several types of GNRs using density functional theory. We have calculated the edge formation free energy in the presence of the adsorbates at the different edges and shown that passivation by atomic oxygen is the most stable closely followed by the hydrogen passivated GNRs. In contrast to the hydrogen saturated zig-zag edge, passivation by oxygen leads

to a non-magnetic and metallic groundstate.

For the vibrational properties, the comparable masses of oxygen and carbon lead to a larger degree of mixing between localized edge and bulk modes. In particular, it is found that the oxygen atoms act as a continuation of the carbon system and participates actively in the longitudinal and out-of-plane series. Only the stretching (transverse) mode of the carbon-oxygen bond is found to be completely localized at the edge and separated from the normal mode series.

Since  $O_2$  and  $H_2$  are almost always present under realistic conditions, our results suggest that it might be very difficult to functionalize the edge atoms with different species. We suggest that the substitutional route, for example via electrothermal reactions as demonstrated in<sup>27</sup>, might turn out to be an easier approach for doping GNRs.

## VI. ACKNOWLEDGMENTS

The authors acknowledge support from the Danish Center for Scientific Computing. The Center for Atomic-scale Materials Design is sponsored by the Lundbeck Foundation.

- 
- <sup>1</sup> K. S. Novoselov, A. K. Geim, S. V. Morozov, D. Jiang, Y. Zhang, S. V. Dubonos, I. V. Grigorieva, A. A. Firsov, *Science* **306**, 666 (2004).
  - <sup>2</sup> K. S. Novoselov, A. K. Geim, S. V. Morozov, D. Jiang, M. Katnelson, I. V. Grigorieva, S. V. Dubonos, A. A. Firsov, *Nature* **438**, 197 (2005).
  - <sup>3</sup> A. K. Geim, K. S. Novoselov, *Nature Mater.* **6**, 183 (2007).
  - <sup>4</sup> A. H. Castro Neto, F. Guinea, N. M. R. Peres, K. S. Novoselov, A. K. Geim, *Rev. Mod. Phys.* **81**, 109 (2009).
  - <sup>5</sup> X. Wang, Y. Ouyang, X. Li, H. Wang, J. Guo, H. Dai, *Phys. Rev. Lett.* **100**, 206803 (2008).
  - <sup>6</sup> X. Li, X. Wang, L. Zhang, S. Lee, H. Dai, *Science* **319**, 1229 (2008).
  - <sup>7</sup> K. A. Ritter, J. W. Lyding, *Nature Mater.* **8**, 235 (2009).
  - <sup>8</sup> P. Koskinen, S. Malola, H. Häkkinen, *Phys. Rev. Lett.* **101**, 115502 (2008).
  - <sup>9</sup> T. Wassmann, A. P. Seitsonen, A. M. Saitta, M. Lazzeri, F. Mauri, *Phys. Rev. Lett.* **101**, 096402 (2008).
  - <sup>10</sup> Er-jun Kan, Z. Li, J. Yang, J. G. Hou, *J. Am. Chem. Soc.* **130**, 4224 (2008).
  - <sup>11</sup> F. Cervantes-Sodi, G. Csányi, S. Piscanec, A. C. Ferrari, *Phys. Rev. B* **77**, 165427 (2008).
  - <sup>12</sup> G. Giovannetti, P. A. Khomyakov, G. Brocks, V. M. Karpan, J. van den Brink, P. J. Kelly, *Phys. Rev. Lett.* **101**, 026803 (2008).
  - <sup>13</sup> M. Vanin, J. J. Mortensen, A. K. Kelkkanen, J. M. Lastra, K. S. Thygesen, K. W. Jacobsen, *Phys. Rev. B* **81**, 081408 (2010).
  - <sup>14</sup> J. J. Mortensen, L. B. Hansen, K. W. Jacobsen, *Phys. Rev. B* **71**, 035109 (2005).
  - <sup>15</sup> J. Enkovaara *et al.*, *J. Phys. Cond. Matt.* **22**, 253202 (2010).
  - <sup>16</sup> P. E. Blöchl, *Phys. Rev. B* **50**, 17953 (1994).
  - <sup>17</sup> B. Hammer, L. B. Hansen, J. K. Nørskov, *Phys. Rev. B* **59**, 7413 (1999).
  - <sup>18</sup> J. K. Nørskov, J. Rossmeisl, A. Logadottir, L. Lindqvist, J. K. Kitchin, T. Bligaard, H. Jónsson, *J. Phys. Chem. B* **108**, 17886 (2004).
  - <sup>19</sup> G. Lee, K. Cho, *Phys. Rev. B* **79**, 165440 (2009).
  - <sup>20</sup> D. Jiang, B. G. Sumpter, S. Dai, *J. Chem. Phys. B* **126**, 134701 (2007).
  - <sup>21</sup> T. Wassmann, A. P. Seitsonen, A. M. Saitta, M. Lazzeri, F. Mauri, *Phys. Status Solidi B* **246**, 2586 (2009).
  - <sup>22</sup> G. Lee, B. Lee, J. Kim, K. Cho *J. Phys. Chem. C* **113**, 14225 (2009).
  - <sup>23</sup> A. P. Seitsonen, A. M. Saitta, T. Wassmann, M. Lazzeri, F. Mauri, *Phys. Rev. B* **82**, 115425 (2010).
  - <sup>24</sup> C. Casiraghi, A. Hartschuh, H. Qian, S. Piscanec, C. Georgi, A. Fasoli, K. S. Novoselov, D. M. Basko, A. C. Ferrari, *Nano Lett.* **9**, 1433 (2009).
  - <sup>25</sup> C. Cong, T. Yu, H. Wang, *ACS Nano* **4**, 3175 (2010).
  - <sup>26</sup> R. Gillen, M. Mohr, C. Thomsen, J. Maultzsch, *Phys. Rev. B* **80**, 155418 (2009).
  - <sup>27</sup> X. Wang, X. Li, L. Zhang, Y. Yoon, P.K. Weber, H. Wang, J. Guo, H. Dai, *Science* **324**, 768 (2009).